Langmuir

Article

pubs.acs.org/Langmuir

Quantitative Contact Resonance Force Microscopy for Viscoelastic Measurement of Soft Materials at the Solid−Liquid Interface

Allison B. Churnside,[†] Ryan C. Tung,[‡] and Jason P. Killgore*,[†]

[†]Applied Chemicals and Materials Division, National Institute of Standards and Technology, 325 Broadway, Mailstop 647, Boulder, Colorado 80305, United States

[‡]Department of Mechanical Engineering, MS 312, University of Nevada, Reno, 1664 N. Virginia Street, Reno, Nevada 89667-0312, United States

Supporting Information

ABSTRACT: Viscoelastic property measurements made at the solid−liquid interface are key to characterizing materials for a variety of biological and industrial applications. Further, nanostructured materials require nanoscale measurements. Here, material loss tangents (tan δ) were extracted from confounding liquid effects in nanoscale contact resonance force microscopy (CR-FM), an atomic force microscope based technique for observing mechanical properties of surfaces. Obtaining reliable CR-FM viscoelastic measurements in liquid is complicated by two effects. First, in liquid, spurious signals arise during cantilever excitation. Second, it is challenging to separate changes to cantilever behavior due to the sample from changes due to environmental damping and added mass effects. We overcame these challenges by applying photothermal cantilever excitation in multiple resonance modes and a predictive model for the hydrodynamic effects. We demonstrated quantitative, nanoscale viscoelastic CR-FM measurements of polymers at the solid−liquid interface. The technique is demonstrated on a point-by-point basis on polymer samples and while imaging in contact mode on a fixed plant cell wall. Values of tan δ for measurements made in water agreed with the values for measurements in air for some experimental conditions on polystyrene and for all examined conditions on polypropylene.

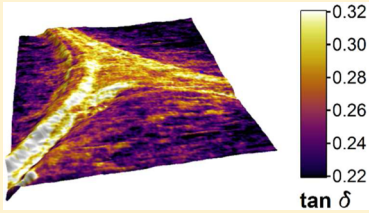

INTRODUCTION

Reliably measuring viscoelasticity in liquid with nanometer spatial resolution remains a difficult problem in the characterization of materials. The elastic and viscoelastic properties of polymer surfaces can vary on nanometer length scales and can change depending on interfaces with fluid. Thus, a number of significant applications would benefit from improved nanoscale quantitative elastic and viscoelastic measurements at the solid−liquid interface, including biological samples, medical materials and devices, and materials for fluid industrial processing. For instance, processing steps for converting plant materials into biofuels often take place in a liquid environment. By understanding how different mutations affect cell wall mechanical properties, feedstock plants could be developed that are easier to handle and process.

Atomic force microscope (AFM)[1] based methods have long demonstrated their sensitivity to elastic and viscoelastic material behavior of surfaces.[2−6] More recent advances have involved applying advanced probing protocols and models to extract quantitative information.[7−10] AFM mechanical property measurements are based on the interaction of a sharp probe with the sample surface. Typically, the probe has a radius of curvature between 5 and 30 nm, resulting in a very small interaction volume suitable for studying nanostructured materials. This small interaction volume also means that the stress field does not extend very far into the material, and AFM probes mostly the surface and interface. The sharp probe is mounted on a soft cantilever, and the deflection is measured optically, allowing measurements to be made with high sensitivity. A large number of AFM-based mechanical property measurement techniques exist, each with advantages and drawbacks.[11] AFM can operate in a wide variety of environments, including in liquid. Operation in liquid can be used to study the effects of solvation and the solid−liquid interface. It also reduces unwanted interactions with hydration layers typically present in ambient environments[7] and increases bandwidth.

Contact resonance force microscopy (CR-FM), a dynamic AFM method, has emerged as a valuable technique for quantitative nanoscale measurements of elasticity and viscoelasticity.[12,13] CR-FM has achieved success at measuring viscoelastic properties of engineered[14] and biological[15,16] surfaces in air and is beginning to measure contact stiffness and qualitatively observe damping at the solid−liquid interface.[17,18] In CR-FM, the resonance properties (resonance frequencies ω and mechanical quality factors Q) of the cantilever are measured when the tip is above and then in contact with the surface. Upon contact with the surface, the free resonance frequencies ω_{free} increase to the contact frequencies ω_{cont}, and the Q values shift from Q_{free} to Q_{cont}. The elastic modulus of the material is a function of the shift in ω, and the loss modulus is a function of both the shift in ω and the change

Received: July 31, 2015
Revised: September 18, 2015
Published: October 1, 2015

DOI: 10.1021/acs.langmuir.5b02860
Langmuir 2015, 31, 11143−11149

in Q. In contrast to subresonant techniques,[4] by making measurements on resonance, the signal is amplified. Operating on resonance also gives access to a number of resonance modes whose dynamic stiffness increases as a function of mode number. Thus, the lower frequency resonance modes can more sensitively measure compliant (low modulus) materials, and the higher frequency modes can more sensitively measure stiff (high modulus) materials.[19,20] Like other AFM techniques, CR-FM is capable of high resolution mapping. Unlike more popular mechanical property measurement techniques based on intermittent contact mode AFM,[3] in CR-FM, the tip is in continuous, dynamic contact with the surface. It has been speculated that continuous contact produces more accurate damping results than intermittent contact by avoiding adhesive effects on the measured signal.[21]

A major obstacle to CR-FM in liquid has been excitation of the cantilever without the spurious resonances introduced by piezoelectric excitation.[22] Particularly when the tip is in contact with the surface, these spurious resonances completely overwhelm the desired cantilever resonance. Direct cantilever excitation by the photothermal method[23,24] avoids these spurious resonances.[18] In this technique, in addition to the typical deflection detection laser, a second laser is focused on the cantilever to periodically heat the top of the cantilever, causing it to bend, and driving cantilever oscillations.

A second major obstacle to quantitative CR-FM in liquid is correctly accounting for the environmental damping and added mass effects from the liquid. During a contact event, the measured change in cantilever behavior depends on the material as well as the environmental properties, which can depend on the distance to the surface. In order to recover the material properties, we must separate out the effects of the fluid environment on the cantilever resonant behavior (Figure 1a).

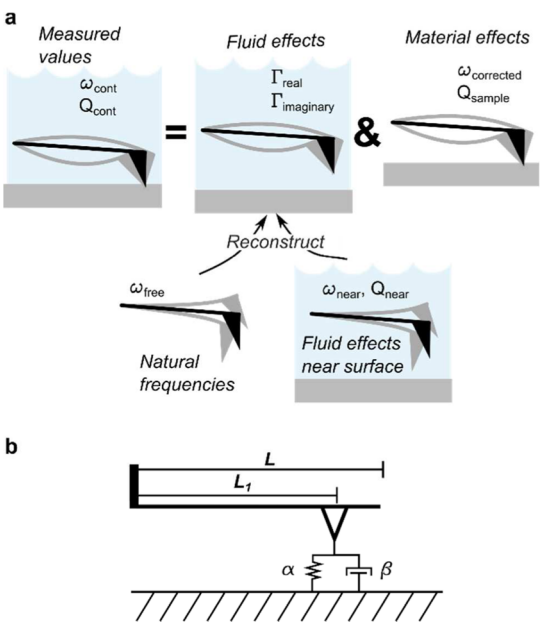

Figure 1. Conceptual drawing of the analysis used to calculate loss tangent. (a) Schematic of the hydrodynamic correction process. The fluid effects are separated from the material effects using a predictive model, which is calibrated by measuring the fluid effect on the cantilever when the cantilever is near the surface. (b) Schematic of the beam model showing L, the total length of the cantilever; L_1, the distance to the tip; α, the contact stiffness; and β, the contact damping.

Then, the fluid contribution to ω_{cont} and Q_{cont} can be estimated and removed from the measured values, leaving $\omega_{corrected}$ and Q_{sample} due only to the interaction of the cantilever with the sample. The contact properties are then determined using a typical spring and dashpot Kelvin−Voigt element (Figure 1b). Recently, our group reported a technique for extracting the fluid background during CR-FM by measuring and reconstructing the hydrodynamic function;[25,26] however, the method was not applied to material property measurements in that work.

In this paper, we report the first nanoscale loss tangent (tan δ) values in water that are shown to agree with those measured in air. To achieve this result, we used photothermal cantilever excitation (BlueDrive, Asylum Research) to obtain contact resonance data in multiple cantilever resonance modes. We demonstrated the method using two common polymers, polystyrene (PS) and polypropylene (PP), whose mechanical properties should be minimally affected by water due to their low absorption of water (supplier specifications: relative mass of water absorbed <0.4% over 24 h for PS and 0.03% at equilibrium for PP). We report that the corrected values agree well with the measurements made in air consistently for PP and under specific experimental conditions for the less damped, and more absorbent, PS. We then demonstrate the applicability of the technique to biological applications by imaging fixed plant cell walls.

■ EXPERIMENTAL SECTION

Data Acquisition during Point Measurements. To excite cantilever resonances, during point measurements the photothermal laser (Blue Drive, Cypher, Asylum Research) was modulated by 1 mW in air and 2 mW in water. Best results for exciting and detecting multiple resonance modes were observed when the excitation and detection laser spots were very close to the base of the cantilever (Supporting Information Figure 1), as expected from cantilever shape during excitation.[27] The cantilever was an aluminum-coated, rectangular cantilever with a nominal spring constant of 2.8 N/m (FMR, Nano World). The drive frequency was swept through the resonance peaks at a rate of 5−40 kHz/s in air and 40−300 kHz/s in water, depending on the width of the peak under examination, and resonance peaks were acquired in 2 s. The frequency sweep width was adjusted to the maximum frequency range that avoided distortion. For PS and PP, data were acquired at multiple locations on each material, alternating between materials after approximately every nine points on a sample containing regions of PS and PP (see Supporting Information: Sample Preparation). Point contact data were collected at approximately 50 nN normal force, and the tip−sample interaction was allowed to settle for 30 s before acquisition of each set of points. For noncontact, near-surface data collection, the cantilever was positioned near the surface by first touching the surface with the cantilever and then retracting the cantilever by approximately 100−200 nm. Because this distance is less than 2% of the height of the tip, the distance between the cantilever and the surface is very similar for the contact measurement and the near-surface measurement. Thus, the hydrodynamics should be similar as well once we correct for frequency and vibrational shape effects.

Data Acquisition during Imaging. For imaging, we again used an aluminum-coated, rectangular cantilever with a nominal spring constant of 2.8 N/m (FMR, Nano World). During imaging, the photothermal laser was modulated by 6 mW, at two frequencies near the resonance, separated by 25 kHz. The sample was scanned at 1 Hz, with an applied force of approximately 50 nN. The raw amplitude and phase data measured during DART tracking were analyzed with a simple harmonic oscillator model in the AFM software to determine ω and Q.[13,28,29]

Data Fitting for Point Measurements. Each resonance peak was fitted to the sum of a damped harmonic oscillator and a linear baseline:

DOI: 10.1021/acs.langmuir.5b02860
Langmuir 2015, 31, 11143−11149

$$A(\omega) = \frac{A_{max}}{Q}\frac{{\omega_0}^2}{\sqrt{({\omega_0}^2 - \omega^2) + \omega^2(\omega_0/Q)^2}} + A_0 + m\omega \quad (1)$$

where A_{max} is the resonance peak height, ω_0 is the resonance frequency, and $A_0 + m\omega$ is the baseline noise.

Estimation of Hydrodynamic Function. To recover the material properties from a measurement made in a fluid, the hydrodynamic effects must be estimated and removed. The hydrodynamic functions Γ_{real} (corresponding to mass loading) and $\Gamma_{imaginary}$ (corresponding to environmental damping) at ω_0 near the surface are readily measured ($\Gamma_{real}(\omega_0)$ and $\Gamma_{imaginary}(\omega_0)$). However, these function values are a poor estimate for the environmental damping in contact since the hydrodynamic functions are frequency dependent (Figure 2), and the resonance frequency shifts upon contact. Therefore, we estimated the hydrodynamic effect at ω_{cont} by interpolating Γ_{real} and $\Gamma_{imaginary}$ measured near the surface to the contact frequencies.[25,26]

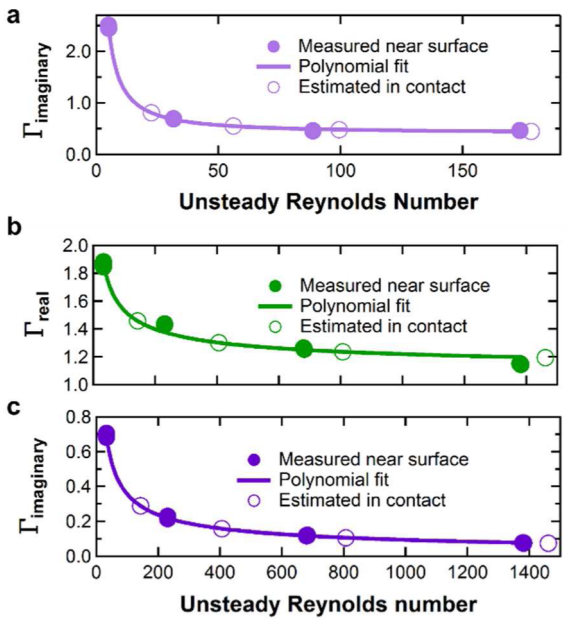

Figure 2. Hydrodynamic function estimates used to analyze the PS and PP data in this paper plotted against unsteady Reynolds number (which is proportional to ω). Solid circles show the hydrodynamic function measured at the first four free resonance frequencies, lines represent the fits to eqs 5 and 6, and open circles are the calculated values of the hydrodynamic function for the first four resonance frequencies during one event when the tip was in contact with PP. (a) Imaginary part of the hydrodynamic function in air. The real part was not used because the effect is negligible. (b) Real part of the hydrodynamic function in water. (c) Imaginary part of the hydrodynamic function in water.

To estimate the hydrodynamic function, we measured the cantilever resonant properties at the first four modes near the surface. Values for Γ_{real} and $\Gamma_{imaginary}$ (Figure 2, solid circles) were determined from

$$\Gamma_r = \frac{(\omega_{free}/\omega_{near})^2 - 1}{\chi} \quad (2)$$

and

$$\Gamma_i = \frac{(\omega_{free}/\omega_{near})^2}{Q_{near}\chi} \quad (3)$$

where ω_{near} and Q_{near} are the resonance properties near the surface, and the dimensionless parameter $\chi = (\pi/4)(\rho_{fluid}b^2/\rho A)$, with ρ and ρ_{fluid} the densities of the cantilever and the fluid, respectively, b the width of the cantilever, and A its cross-sectional area. The real and imaginary parts of the hydrodynamic function are plotted as a function of unsteady Reynolds number Re

$$Re = \frac{\rho_{fluid}}{4\mu_{fluid}}b^2\omega \quad (4)$$

where μ_{fluid} is the shear viscosity of the fluid.

We fit the near-surface hydrodynamic functions to a polynomial expansion. By using an asymptotic expansion for the functional form of the hydrodynamic function for a long slender beam,[25,30] we can determine the order of the first few terms and insert fitting coefficients a, b, and c to fit the data near the surface, namely

$$\Gamma_r = a_1 + b_1 Re^{-1/2} \quad (5)$$

and

$$\Gamma_i = a_2 + b_2 Re^{-1/2} + c_2 Re^{-1} \quad (6)$$

Application of Hydrodynamic Correction. By applying the reconstructed hydrodynamic correction, we can determine the equivalent in-air ω_{cont} and Q_{cont} and thus separate sample properties from environmental effects. Application of the hydrodynamic function is described in more detail elsewhere.[25,26] After the real and imaginary parts of the reconstructed hydrodynamic function Γ_r and Γ_i were determined at the contact frequencies from eqs 5 and 6, the corrected contact frequencies were calculated from

$$\omega_{corrected} = \omega_{measured}[1 + \chi\Gamma_r(Re_{\omega_{cont}})]^{1/2} \quad (7)$$

The fluid damping was calculated with

$$Q_{fluid} = \frac{\chi^{-1} + \Gamma_r(Re_{\omega_{cont}})}{\Gamma_i(Re_{\omega_{cont}})} \quad (8)$$

and the damping from contact with the sample is then given by

$$\frac{1}{Q_{sample}} = \frac{1}{Q_{measured}} - \frac{1}{Q_{fluid}} \quad (9)$$

where $Q_{measured}$ is the uncorrected quality factor obtained from fitting the resonance peak in contact with the surface.

Calculation of Loss Tangent. Unlike the storage and loss moduli, tan δ does not depend on the contact geometry, thus avoiding a major source of uncertainty.[15] The loss tangent tan δ was computed directly from the equation[25]

$$\tan\delta = \frac{(\lambda L)^2\beta}{\alpha}\left(\frac{L_1}{L}\right)^2\frac{\omega}{\omega_{free}} \quad (10)$$

where α and β are the tip−surface contact stiffness and damping coefficient, respectively, determined as described elsewhere, and ω is ω_{cont} for uncorrected results and $\omega_{corrected}$ for corrected data.[13] These parameters α and β depend on the free resonance frequency ω_{free}, the contact resonance frequency ω_{cont} or $\omega_{corrected}$, and the sample mechanical quality factor Q_{sample}.

The parameters α and β also depend on the position of the tip L_1/L along the cantilever. Although L_1/L could in principle be determined optically, it is typically[31] determined by examining a data set containing contact resonance frequencies for multiple eigenmodes during a single contact event. Contact stiffness should depend minimally on frequency; thus, L_1/L can be treated as an adjustable parameter to give equal contact stiffness values for multiple eigenmodes (Supporting Information Figure 2 and Table 1). Because L_1/L represents a geometric parameter, CR-FM results in air were used for this step regardless of environment. Average values for the crossing between modes 1 and 2 were used to calculate tan δ for mode 1, average values for the crossing between modes 2 and 3 were used to calculate tan δ for mode 2, and average values for the crossing between modes 3 and 4 were used calculate tan δ for modes 3 and 4.

DOI: 10.1021/acs.langmuir.5b02860
Langmuir 2015, 31, 11143−11149

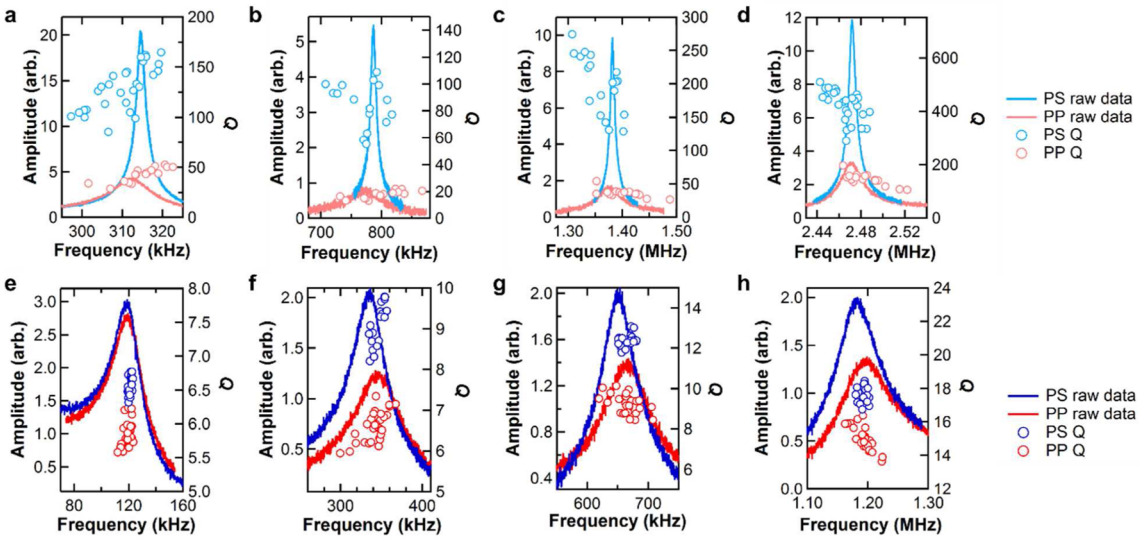

Figure 3. Data collected using photothermally excited cantilever. Shown are frequency sweeps for a representative contact event (lines) and Q values extracted from all contact events (circles). (a−d) In air, PS (light blue) and PP (pink) resonance peaks display a large contrast in Q between materials. (e−h) In water, the fluid damping dominates, so that the differences between PS (blue) and PP (red) and the Q contrast are more subtle.

Table 1. Values for tan δ Measured in Air and in Water with and without the Hydrodynamic Correction[a]

PP	mode 1	mode 2	mode 3	mode 4
air, corrected	0.18 ± 0.03, N = 17	0.09 ± 0.02, N = 15	0.10 ± 0.01, N = 16	0.08 ± 0.01, N = 17
water, uncorrected	0.46 ± 0.08, N = 31	0.17 ± 0.01, N = 31	0.15 ± 0.02, N = 30	0.16 ± 0.02, N = 31
water, corrected	0.03 ± 0.01, N = 31	0.11 ± 0.01, N = 31	0.12 ± 0.02, N = 30	0.10 ± 0.01, N = 31
error reduction	1.9	4	2.5	4
PS	mode 1	mode 2	mode 3	mode 4
air, corrected	0.035 ± 0.008, N = 28	0.020 ± 0.005, N = 16	0.017 ± 0.004, N = 20	0.018 ± 0.006, N = 29
water, uncorrected	0.44 ± 0.04, N = 19	0.088 ± 0.008, N = 19	0.064 ± 0.007, N = 19	0.08 ± 0.01, N = 19
water, corrected	−0.02 ± 0.01, N = 19	0.03 ± 0.01, N = 19	0.038 ± 0.006, N = 19	0.04 ± 0.01, N = 19
error reduction	7.4	6.8	2.2	2.8

[a]Results are shown as (mean value ± standard deviation), with the number of data points N as shown. The error reduction for each case is given by $|(\tan(\delta)_{\text{uncorrected}} - \tan(\delta)_{\text{air}})/(\tan(\delta)_{\text{corrected}} - \tan(\delta)_{\text{air}})|$.

■ RESULTS AND DISCUSSION

Photothermal excitation of the cantilever produced contact resonance peaks that were free of spurious resonances and had the expected Lorentzian shape for the first four flexural modes in air and in water (Figure 3). The incident laser power of 10 mW was not observed to unduly affect the resonance characteristics of the cantilever (Supporting Information Figure 3 and Table 2). Photothermal excitation thus provides the ability to simultaneously measure multiple resonance modes in contact in two very different environments. In contrast with thermal excitation,[26] these measurements can be made quickly, minimizing artifacts due to drift and allowing imaging.

Qualitative examination of representative contact events (Figure 3, lines) and all fitted Q values (Figure 3, circles) demonstrates the decrease in material contrast when operating in water. From bulk dynamic mechanical analysis (DMA) measurements, PS is expected to exhibit a loss tangent which is approximately a factor of 10 smaller than PP. This disparity in material damping can be seen in the pronounced difference in peak width between PS (Figure 3a−d, light blue) and PP (Figure 3a−d, pink). The measured Q values are also clearly different depending on material. In water, however, the peaks on both materials appear highly damped (Figure 3e−h), reducing the apparent differences between materials, and the Q values measured on PS are more similar to those measured on PP.

For both materials, corrected values of tan δ in air (Table 1) are near the expected values of approximately 0.01 for PS[12] and 0.1 for PP (DMA, data not shown). For data in air, tan δ was calculated using ω_{free} in air, $\omega_{\text{corrected}}$ in air, and Q_{sample} in air. The Γ_{real} is negligible in air,[25] so only $\Gamma_{\text{imaginary}}$ (Figure 2a) was used.

Using an uncorrected value for the environmental damping in water results in overestimated tan δ values. Furthermore, it results in underestimated tan δ ratios between materials (material contrast) by at least a factor of 2 (Table 1). The largest absolute discrepancy and smallest relative contrast were observed for mode 1. The damping response of the cantilever in mode 1 is dominated by the fluid properties rather than sample properties as expected from the rapidly increasing hydrodynamic function when moving toward a lower frequency (Figure 2b,c). Although the values do not agree with the air values without correction, the expected rank order in tan δ was preserved in modes 2−4. This demonstrates that under the correct conditions qualitative rank measurements may be made in liquids without hydrodynamic reconstruction, and contrast can be enhanced by selecting higher resonant modes.

Using the reconstructed hydrodynamic function, tan δ measured in water agreed significantly better with tan δ

DOI: 10.1021/acs.langmuir.5b02860
Langmuir 2015, 31, 11143−11149

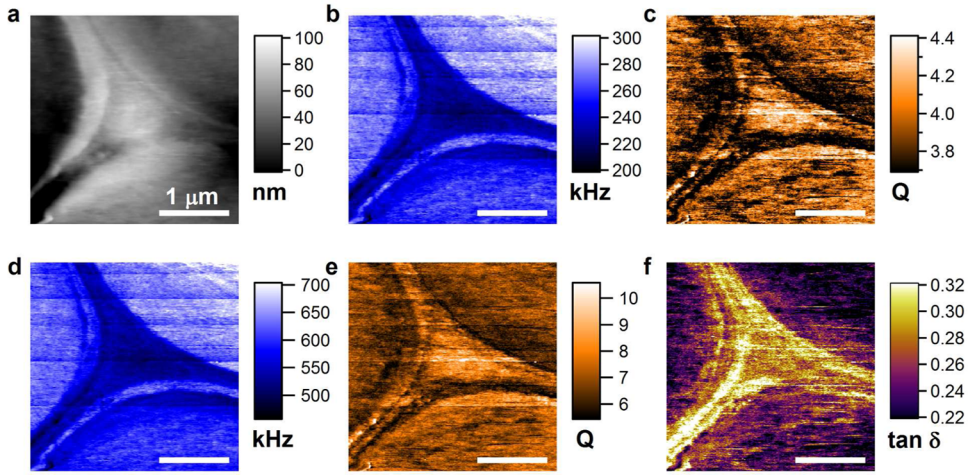

Figure 4. Loss tangent imaged in mode 2 on *Arabidopsis thaliana* plant cell walls in water. (a) Height image, smoothed by a 3 × 3 pixel median filter. (b) Raw contact resonance frequency. (c) Raw contact resonance Q. (d) Contact resonance frequency after hydrodynamic correction. (e) Q after hydrodynamic correction showing improvement in dynamic range over raw Q. (f) Loss tangent calculated from corrected values.

measured in air (Table 1). For corrected data in water, the tan δ was calculated using ω_{free} in air, $\omega_{corrected}$ in water, and Q_{sample} in water. The reduction in error by the reconstructed hydrodynamic function $|(\tan(\delta)_{uncorrected} - \tan(\delta)_{air})/(\tan(\delta)_{corrected} - \tan(\delta)_{air})|$ ranged from a factor of 2 to a factor of 7 depending on mode and material.

In mode 1, the hydrodynamic reconstruction overcorrected tan δ, leading to an unphysical negative value on PS. This is likely due to increased error in estimating the hydrodynamic function. At lower frequency, the hydrodynamic function is more frequency dependent. Additionally, instrumental noise is greater at low frequency, apparent from the tilted baseline in the data (Figure 3e). Furthermore, the beam model used to determine the stiffness of the spring and damping of the dashpot is most accurate when the dynamic stiffness of the chosen vibrational mode matches the stiffness of the surface. Since dynamic stiffness increases with mode number, in this case higher modes are better matched to the sample.

PS, having lower tan δ, is expected to be more sensitive to uncertainty in measuring liquid damping. Indeed, tan δ for PS measured in water agreed with the value measured in air only in mode 2. The value of tan δ was overestimated in subsequent modes, although the error was significantly reduced compared to the uncorrected case. The hydrodynamic reconstruction works less effectively at higher modes because it is based on a two-dimensional model for the cantilever, which becomes less valid for the higher resonance modes where axial flow of the liquid becomes significant.[32] In modes 2−4 on PP, tan δ measured in water agreed with that measured in air to within experimental error, showing the high accuracy of the method when applied to more dissipative materials.

To demonstrate the technique during imaging of a biological sample in water, we imaged a fixed sample of *Arabidopsis thaliana* cell walls (see Supporting Information: Sample Preparation). A comparison between hydrodynamic functions measured near the plant cell walls to those measured near PS shows near-perfect agreement (Supporting Information Figure 4), lending confidence in the ability of the technique to extend from hydrophobic, low-swelling materials to biological samples. Figure 4 shows a junction between three cells imaged using the dual ac resonance tracking (DART) technique.[13,28,29] Based on the results from the PP and PS sample, mode 2 of the cantilever was observed during scanning to acquire this image. The corrected Q in Figure 4e displays an expanded range and therefore improved contrast in Q compared to the raw Q in Figure 4c. Horizontal artifacts can be seen in Figure 4b−e. These are likely due to variations in tip−sample contact area, as they are less apparent in the loss tangent (Figure 4f), which is insensitive to contact area. Contrast in the loss tangent can be seen between primary cell walls, secondary cell walls, and the middle lamella. The calculated values for tan δ are similar to those previously reported for cellulosic plant matter.[33,34] These data show the practicality of the technique for quantitative viscoelastic imaging at the solid−liquid interface.

■ CONCLUSION

By more accurately estimating the fluid added mass and damping, we have demonstrated surface tan δ measured with a nanoscale probe in water in agreement with similar measurements in air, to our knowledge for the first time. The technique provides robust agreement on a higher loss materials (tan δ > 0.1) for all measured modes except mode 1. This reveals the first criterion for accurate CR-FM loss tangent measurements in liquid: choose a resonance mode that avoids the steepest part of the hydrodynamic function. On a lower loss material (tan $\delta \approx$ 0.01) where environmental damping is more dominant, the best agreement was found using mode 2. This avoids the pitfalls of mode 1 mentioned above, while also avoiding the slight loss in accuracy of the hydrodynamic function with increasing frequency that occurs due to unaccounted-for three-dimensional flow. Other key considerations include matching the stiffness of the cantilever mode to the contact stiffness, the positioning of the excitation and detection lasers, and the speed of the frequency sweep (see Supporting Information: Methods). Our result demonstrates that tan δ of surfaces in water can be accurately measured. The method can also be applied simultaneously with liquid contact-mode imaging to produce spatially resolved viscoelastic maps. Overall, the method allows characterization of materials in a variety of critical biological and industrial applications where measurements in air are not appropriate or available.

DOI: 10.1021/acs.langmuir.5b02860
Langmuir 2015, 31, 11143−11149

■ ASSOCIATED CONTENT

Supporting Information

The Supporting Information is available free of charge on the ACS Publications website at DOI: 10.1021/acs.langmuir.5b02860.

Optimal positioning of excitation and detection lasers, determination of effective tip position along cantilever, resonance behavior with and without excitation laser on, comparisons of hydrodynamic functions measured near different substrates, sample preparation (PDF)

■ AUTHOR INFORMATION

Corresponding Author

*E-mail Jason.Killgore@nist.gov (J.P.K.).

Funding

This work was funded by NIST and by National Research Council Research Associateship awards to A.B.C. and R.C.T.

Notes

The authors declare no competing financial interest.

■ ACKNOWLEDGMENTS

The authors thank Dr. Christian Long (NIST) for a valuable experimental insight, Lewis Cox (University of Colorado) for DMA measurements, Dr. Peter Ciesielski (NREL) for *Arabidopsis* samples, and Dr. Ryan Wagner (NIST) for technical assistance. Certain commercial materials and supplies are identified in this paper to foster understanding. Such identification does not imply recommendation or endorsement by the National Institute of Standards and Technology, nor does it imply that the materials or equipment identified are necessarily the best available for the purpose. This document is an official contribution of the National Institute of Standards and Technology, and not subject to copyright in the United States.

■ REFERENCES

(1) Binnig, G.; Quate, C.; Gerber, C. Atomic force microscope. *Phys. Rev. Lett.* **1986**, *56*, 930−933.

(2) Burnham, N. A.; Colton, R. J. Measuring the nanomechanical properties and surface forces of materials using an atomic force microscope. *J. Vac. Sci. Technol., A* **1989**, *7* (4), 2906−2913.

(3) Tamayo, J.; Garcia, R. Deformation, contact time, and phase contrast in tapping mode scanning force microscopy. *Langmuir* **1996**, *12* (18), 4430−4435.

(4) Radmacher, M.; Tillmann, R.; Gaub, H. Imaging viscoelasticity by force modulation with the atomic force microscope. *Biophys. J.* **1993**, *64* (3), 735−742.

(5) Kajiyama, T.; Tanaka, K.; Ohki, I.; Ge, S.-R.; Yoon, J.-S.; Takahara, A. Imaging of dynamic viscoelastic properties of a phase-separated polymer surface by forced oscillation atomic force microscopy. *Macromolecules* **1994**, *27* (26), 7932−7934.

(6) Benmouna, F.; Johannsmann, D. Viscoelasticity of gelatin surfaces probed by AFM noise analysis. *Langmuir* **2004**, *20* (1), 188−193.

(7) Chyasnavichyus, M.; Young, S. L.; Tsukruk, V. V. Probing of polymer surfaces in the viscoelastic regime. *Langmuir* **2014**, *30* (35), 10566−10582.

(8) Pittenger, B.; Erina, N.; Su, C. Mechanical property mapping at the nanoscale using PeakForce QNM scanning probe technique. In *Nanomechanical Analysis of High Performance Materials*, Tiwari, A., Ed.; Springer: Dordrecht, 2014; pp 31−51.

(9) Garcia, R.; Proksch, R. Nanomechanical mapping of soft matter by bimodal force microscopy. *Eur. Polym. J.* **2013**, *49* (8), 1897−1906.

(10) Wang, D.; Liang, X.-B.; Liu, Y.-H.; Fujinami, S.; Nishi, T.; Nakajima, K. Characterization of surface viscoelasticity and energy dissipation in a polymer film by atomic force microscopy. *Macromolecules* **2011**, *44* (21), 8693−8697.

(11) Chyasnavichyus, M.; Young, S. L.; Tsukruk, V. V. Recent advances in micromechanical characterization of polymer, biomaterial, and cell surfaces with atomic force microscopy. *Jpn. J. Appl. Phys.* **2015**, *54* (8S2), 08LA02.

(12) Hurley, D. C.; Campbell, S. E.; Killgore, J. P.; Cox, L. M.; Ding, Y. Measurement of Viscoelastic Loss Tangent with Contact Resonance Modes of Atomic Force Microscopy. *Macromolecules* **2013**, *46* (23), 9396−9402.

(13) Killgore, J.; Yablon, D.; Tsou, A.; Gannepalli, A.; Yuya, P.; Turner, J.; Proksch, R.; Hurley, D. Viscoelastic property mapping with contact resonance force microscopy. *Langmuir* **2011**, *27* (23), 13983−13987.

(14) Yuya, P.; Hurley, D.; Turner, J. A. Contact-resonance atomic force microscopy for viscoelasticity. *J. Appl. Phys.* **2008**, *104* (7), 074916.

(15) Campbell, S. E.; Ferguson, V. L.; Hurley, D. C. Nanomechanical mapping of the osteochondral interface with contact resonance force microscopy and nanoindentation. *Acta Biomater.* **2012**, *8* (12), 4389−4396.

(16) Ciesielski, P. N.; Resch, M. G.; Hewetson, B.; Killgore, J. P.; Curtin, A.; Anderson, N.; Chiaramonti, A. N.; Hurley, D. C.; Sanders, A.; Himmel, M. E. Engineering plant cell walls: tuning lignin monomer composition for deconstructable biofuel feedstocks or resilient biomaterials. *Green Chem.* **2014**, *16* (5), 2627−2635.

(17) Parlak, Z.; Tu, Q.; Zauscher, S. Liquid contact resonance AFM: analytical models, experiments, and limitations. *Nanotechnology* **2014**, *25* (44), 445703.

(18) Kocun, M.; Labuda, A.; Gannepalli, A.; Proksch, R. Contact resonance atomic force microscopy imaging in air and water using photothermal excitation. *Rev. Sci. Instrum.* **2015**, *86* (8), 083706.

(19) Turner, J. A.; Wiehn, J. S. Sensitivity of flexural and torsional vibration modes of atomic force microscope cantilevers to surface stiffness variations. *Nanotechnology* **2001**, *12* (3), 322.

(20) Killgore, J. P.; Hurley, D. C. Low-force AFM nanomechanics with higher-eigenmode contact resonance spectroscopy. *Nanotechnology* **2012**, *23* (5), 055702.

(21) Yablon, D. G.; Grabowski, J.; Chakraborty, I. Measuring the loss tangent of polymer materials with atomic force microscopy based methods. *Meas. Sci. Technol.* **2014**, *25* (5), 055402.

(22) Xu, X.; Raman, A. Comparative dynamics of magnetically, acoustically, and Brownian motion driven microcantilevers in liquids. *J. Appl. Phys.* **2007**, *102* (3), 034303.

(23) Ratcliff, G. C.; Erie, D. A.; Superfine, R. Photothermal modulation for oscillating mode atomic force microscopy in solution. *Appl. Phys. Lett.* **1998**, *72* (15), 1911−1913.

(24) Umeda, N.; Ishizaki, S.; Uwai, H. Scanning attractive force microscope using photothermal vibration. *J. Vac. Sci. Technol., B* **1991**, *9* (2), 1318−1322.

(25) Tung, R. C.; Killgore, J. P.; Hurley, D. C. Hydrodynamic corrections to contact resonance atomic force microscopy measurements of viscoelastic loss tangent. *Rev. Sci. Instrum.* **2013**, *84* (7), 073703.

(26) Tung, R. C.; Killgore, J. P.; Hurley, D. C. Liquid contact resonance atomic force microscopy via experimental reconstruction of the hydrodynamic function. *J. Appl. Phys.* **2014**, *115* (22), 224904.

(27) Wagner, R.; Killgore, J. P.; Tung, R. C.; Raman, A.; Hurley, D. C. Vibrational shape tracking of atomic force microscopy cantilevers for improved sensitivity and accuracy of nanomechanical measurements. *Nanotechnology* **2015**, *26* (4), 045701.

(28) Rodriguez, B. J.; Callahan, C.; Kalinin, S. V.; Proksch, R. Dual-frequency resonance-tracking atomic force microscopy. *Nanotechnology* **2007**, *18* (47), 475504.

(29) Gannepalli, A.; Yablon, D.; Tsou, A.; Proksch, R. Mapping nanoscale elasticity and dissipation using dual frequency contact resonance AFM. *Nanotechnology* **2011**, *22* (35), 355705.

DOI: 10.1021/acs.langmuir.5b02860
Langmuir 2015, 31, 11143−11149

(30) Tuck, E. Calculation of unsteady flows due to small motions of cylinders in a viscous fluid. *J. Eng. Math.* **1969**, *3* (1), 29−44.
(31) Rabe, U.; Amelio, S.; Kester, E.; Scherer, V.; Hirsekorn, S.; Arnold, W. Quantitative determination of contact stiffness using atomic force acoustic microscopy. *Ultrasonics* **2000**, *38* (1), 430−437.
(32) Van Eysden, C. A.; Sader, J. E. Frequency response of cantilever beams immersed in viscous fluids with applications to the atomic force microscope: Arbitrary mode order. *J. Appl. Phys.* **2007**, *101* (4), 044908.
(33) Zhang, T.; Bai, S. L.; Zhang, Y. F.; Thibaut, B. Viscoelastic properties of wood materials characterized by nanoindentation experiments. *Wood Sci. Technol.* **2012**, *46* (5), 1003−1016.
(34) Havimo, M. A literature-based study on the loss tangent of wood in connection with mechanical pulping. *Wood Sci. Technol.* **2009**, *43* (7−8), 627−642.

DOI: 10.1021/acs.langmuir.5b02860
Langmuir 2015, 31, 11143−11149